Nanoscale

Bottom-up Meets Top-down: Tailored Raspberry-like Fe_3O_4-Pt Nanocrystal Superlattices

Journal:	*Nanoscale*
Manuscript ID	NR-COM-01-2018-000655.R1
Article Type:	Communication
Date Submitted by the Author:	08-Mar-2018
Complete List of Authors:	Qiu, Fen; Lawrence Berkeley National Laboratory, The Molecular Foundry Vervuurt, René; Technische Universiteit Eindhoven, Applied Physics Verheijen, Marcel; Philips Innovation Services ; Eindhoven University of Technology, Zaia, Edmond; University of California Berkeley Creel, Erin; University of California Berkeley Kim, Youngsang; E O Lawrence Berkeley National Laboratory Urban, Jeffrey; Lawrence Berkeley National Laboratory, Bol, Ageeth; Eindhoven University of Technology, Applied Physics

Journal Name

COMMUNICATION

Bottom-up Meets Top-down: Tailored Raspberry-like Fe_3O_4-Pt Nanocrystal Superlattices

Received 00th January 20xx,
Accepted 00th January 20xx

DOI: 10.1039/x0xx00000x

www.rsc.org/

Fen Qiu,[a †] René H. J. Vervuurt,[b †] Marcel A. Verheijen,[b,c] Edmond W. Zaia,[a,d] Erin B. Creel,[a,d] Youngsang Kim,[a] Jeffrey J. Urban,*[a] Ageeth A. Bol*[b]

Supported catalysts are widely used in industry and can be optimized by tuning the composition, chemical structure, and interface of the nanoparticle catalyst and oxide support. Here we firstly combine a bottom up colloidal synthesis method with a top down atomic layer deposition (ALD) process to achieve a raspberry-like Pt-decorated Fe_3O_4 (Fe_3O_4-Pt) nanoparticle superlattice. This nanocomposite ensures the precision of the catalyst/support interface, improving the catalytic efficiency of the Fe_3O_4-Pt nanocomposite system. The morphology of the hybrid nanocomposites resulting from different cycles of ALD was monitored by scanning transmission electron microscopy, giving insight into the nucleation and growth mechanism of the ALD process. X-ray photoelectron spectroscopy studies confirm the anticipated electron transfer from Fe_3O_4 to Pt through the nanocomposite interface. Photocurrent measurement further suggests that Fe_3O_4 superlattices with controlled decoration of Pt have substantial promise for energy-efficient photoelectrocatalytic oxygen evolution reaction. This work opens a new avenue for designing supported catalyst architectures via precisely controlled decoration of single component superlattices with noble metals.

Hybrid nanocomposites are a rapidly growing field because of their unique optical,[1] catalytic,[2] and electrochemical properties[3] generated through the interactions between each component. Precise control of the structure, size, morphology and interface of these nanocomposites has made it possible to tailor the properties of the nanocomposites for better catalytic activity and selectivity.[4, 5] Supported catalysts composed of noble metals on metal oxide supports have been widely used in catalysis,[6, 7] however, these catalysts are typically not uniform in composition and/or structure. This makes the formation of ordered hierarchical structures with new functionalities based on noble metals/oxide interface a fundamental materials challenge. Driven by a variety of technological applications and global scientific interest, metal oxides can now be routinely synthesized as monodisperse spherical colloids with precise control over the size and morphology even on a large-scale, making it simple to assemble them into single component NP superlattices.[8, 9] The use of binary nanoparticles to form superlattices has been an effective approach to achieve the needed metal–metal oxide interfaces, but the process of assembly remains laborious and difficult to scale to large areas.[10, 11] Alternatively, decorating the single-component superlattices using noble metals with precise and efficient control provides a facile and scalable route to design and fabricate ideal supported catalysts. One technique that offers unique possibilities for the controlled deposition of the noble metal catalyst on oxide support is Atomic Layer Deposition (ALD). The initial stages of noble metal ALD typically deviate from the characteristic layer-by-layer growth due to differences in wetting behavior and catalytic activity of the noble metals.[12] This leads to the formation of noble metal nanoparticles rather than ultrathin films. Due to the self-limiting behavior of ALD, excellent control of the noble metal nanoparticle size can be achieved.[13, 14] In addition, ALD is known for the uniform deposition on 3D structures.[15] Furthermore, ALD of noble metals can be made selective towards catalytic surfaces.[16, 17] ALD is therefore a promising approach for the preparation of noble metal catalysts on metal oxide nanoparticles.

Recently, studies on developing hybrid Pt decorated Fe_3O_4 have either focused on multiple-step, bottom-up, and solution-based syntheses,[18] or top-down deposition of thin-films directly on the substrates. These often result in poor

[a] A Dr. F. Qiu, E. W. Zaia, E. Creel, Dr. Y. King and Dr. J. J. Urban
The Molecular Foundry, Lawrence Berkeley National Laboratory
1 Cyclotron Road, Berkeley, CA, 94720 USA
E-mail: jjurban@lbl.gov.
[b] Dr. R. H. J. Vervuurt, Dr. M. A. Verheijen and Dr. A. A. Bol
Department of Applied Physics, Eindhoven University of Technology, P.O. Box 513, 5600 MB Eindhoven, The Netherlands
E-mail: a.a.bol@tue.nl
[c] Dr. M. A. Verheijen
Philips Innovation Labs, High Tech Campus 11, 5656 AE Eindhoven. The Netherlands
[d] E. W. Zaia, E. Creel
University of California, Berkeley, California 94720, United States
Electronic Supplementary Information (ESI) available: [details of any supplementary information available should be included here]. See DOI: 10.1039/x0xx00000x

control over the material structures and/or high cost due to the large amount of noble metal catalyst required. In this study, we combine a bottom-up colloidal synthesis technique with top-down ALD for the synthesis of Pt decorated Fe_3O_4 (Fe_3O_4-Pt) nanoparticle superstructures. The addition of Pt on the Fe_3O_4 superlattices can be well-controlled by ALD and allows for easy formation of raspberry-like hybrid superstructures (Figure 1b and c). The synthesis process is monitored by scanning transmission electron microscopy (STEM), and the growth mechanism is discussed. The size of the Pt NPs is precisely controlled by the number of deposition cycles. Furthermore, we demonstrate synergistic inter-particle interactions using a combination of X-ray photoelectron spectroscopy (XPS) and photoelectrocatalytic water splitting measurements to reveal the interfacial energetics. This precision design method, combining ALD with colloidal synthesis techniques, opens a new avenue for the engineering of various hybrid catalysts.

The Fe_3O_4 NPs used in this study were synthesized by colloidal synthesis as reported in the literature with slight modification.[9] Large-scale Fe_3O_4 nanoparticle superlattices were formed via assembly at the air-liquid interface.[19] The narrow size distribution of the Fe_3O_4 NPs is demonstrated by the formation of single component superlattices (Figure 1a). The ordered area can be larger than 10 µm, and shows hexagonal symmetry, further confirmed by FFT. (Figure S1). After the transfer of the Fe_3O_4 superlattices to the TEM grids, the Fe_3O_4 NPs were decorated with Pt NPs by ALD. The ALD process took place at 300°C using $MeCpPtMe_3$ as the precursor and O_2 as the co-reactant. It should be noticed that the partial Fe_3O_4 could be oxidized to Fe_2O_3 during the ALD process, although the substrate heater the temperature of the samples is only ~120 °C due to the bad thermal contact between samples and the substrate heater. Figure 1b and 1c confirm the deposition of the Pt NPs. Figure 1b shows a representative hexagonal order of the superlattice has been maintained after ALD, and figure 1c shows good contact between Fe_3O_4 NPs and Pt NPs.

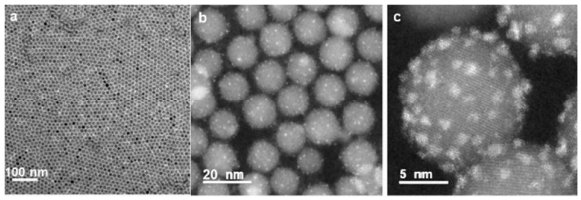

Figure 1. (a) TEM image of Fe_3O_4 Nanoparticle Superlattices formed by air-liquid assembly process, (b) and (c) STEM images of Fe_3O_4-Pt (200 cycles Pt ALD)

In order to study the nucleation and growth mechanism of Pt ALD on Fe_3O_4 NPs, we simply drop casted the Fe_3O_4 NPs on TEM grids. It was observed that this process also leads to the formation of a hexagonal ordered structure, but over a relatively small area (Figure S2). After colloidal self-assembly, the TEM grid was subjected to Pt ALD.

Figure 2 a)- f) shows the Fe_3O_4 particles decorated with Pt as a function of the number of ALD cycles. The Pt NPs have been successfully deposited on the surface of the Fe_3O_4 spheres. The HR-STEM shown in the Fig S3 showed good contact between Fe_3O_4 and Pt NPs. It can be seen that the amount of Pt deposited on the Fe_3O_4 particles increases with cycle numbers up to ~ 100 cycles. After 100 cycles, the amount of Pt deposited on the Fe_3O_4 no longer appears to increase. This indicates that the growth of Pt is inhibited after a certain amount of Pt ALD cycles. This is also confirmed from the size distribution of the particles, determined from the TEM images, shown in Figure 3. Additionally, it was noticed that the average particle size after 30 cycles is larger compared to 50 cycles. This is most likely due to the conversion of 2D Pt islands to 3D particles, once the Pt clusters have reached a certain size. However, this could also be caused by some sample to sample variation leading to small differences in the nucleation delay.

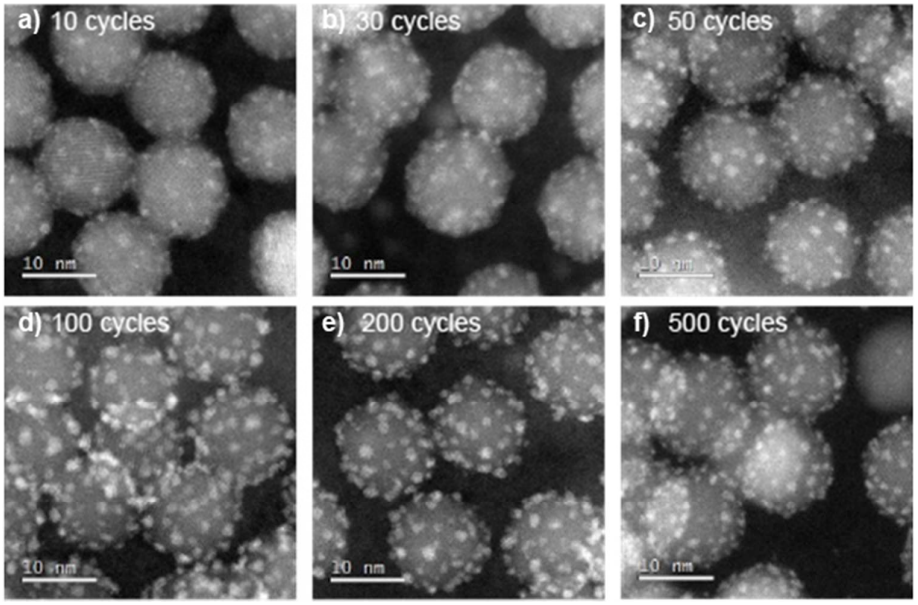

Figure 2. High angle annular dark field (HAADF) scanning transmission electron microscopy (STEM) images of Fe_3O_4 NPs after (a) 10, (b) 30, (c) 50, (d) 100, (e) 200 and (f) 500 Pt ALD cycles respectively.

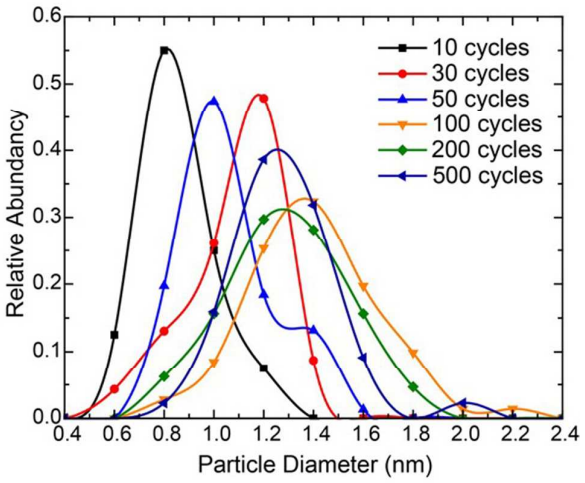

Figure 3. Pt particle size distribution as a function of the number of Pt ALD cycles determined by analyzing the HAADF STEM images. (Analysis of each sample with snapshots taken at different locations of the sample)

The inhibition of the Pt ALD growth after a certain number of ALD cycles could be caused by the poisoning of the growth surface due to the formation of a carbon rich layer on the particles.[20, 21] ALD of Pt NPs proceeds because of the favorable catalytic activity of the Pt nuclei.[12] However, the size of the catalyst NP (in this case Pt) is known to play an important role in its catalytic activity.[22-24] It could therefore be that once the particles have reached a certain size (~1.6 nm), a reaction pathway opens that leads to the poisoning of the Pt particles. This layer could block the adsorption of the $MeCpPtMe_3$ precursor on the existing Pt NPs during prolonged growth. The adsorption of the $MeCpPtMe_3$ precursor on a surface is very sensitive to the presence of organic compounds, which are known to inhibit Pt growth.[25-27] To confirm if the formation of a carbon rich film is indeed the cause for the blocking of the Pt growth, 200 cycles of Pt ALD were performed on several samples with Fe_3O_4 NPs. For some samples, the deposition was interrupted by a short O_2 plasma treatment after every 50 cycles or 100 cycles to remove any carbon that might have formed on the Pt particles. Figure 4 a-c shows that the use of an O_2 plasma to clean the Pt particles after every 50 or 100 cycles results in the deposition of substantially more Pt on the Fe_3O_4 then when the particles are not cleaned once in a while. The O_2 plasma treatments allow for the continued growth of the Pt particles, as can also be observed from the particle size distribution shown in Figure 4d. Interrupting the ALD process every 50 cycles already results in the agglomeration of the Pt particles and the initial stages of the creation of a Pt-shell around the Fe_3O_4 particles. The air-liquid method is better for 2-D self-assembly at larger length scales due to the templating effects naturally present at the interface. However, as we did not notice any effect of self-assembly method on the Pt NP deposition or the photocatalytic activity of the composites, we simply chose the drop casting method for studying the nucleation and growth mechanism of Pt ALD on Fe_3O_4 NPs.

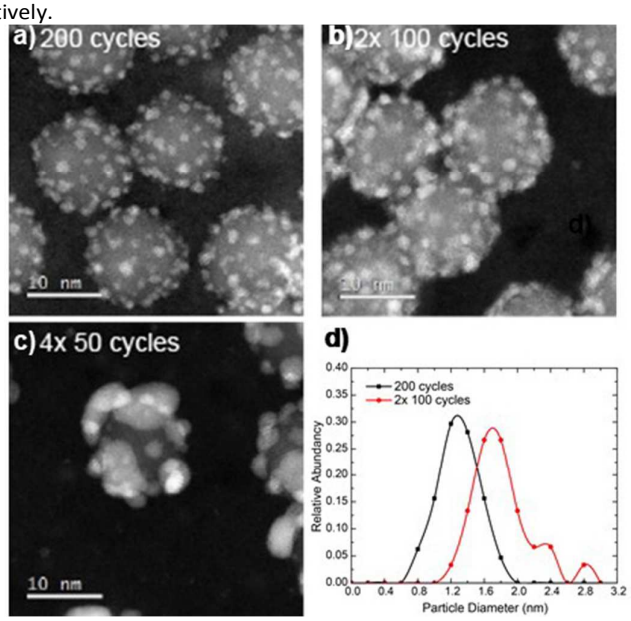

Figure 4. High angle annular dark field (HAADF) scanning transmission electron microscopy (STEM) images of Fe_3O_4 spheres after (a) 200 Pt ALD cycles, (b) 2x 100 ALD cycles separated by an O_2 plasma treatment and (c) 4x 50 cycles separated by an O_2 plasma treatment (d) Pt particle size distribution after 200 Pt ALD cycles and 2x 100 ALD cycles separated by an O_2 plasma treatment. The size distribution is determined from the HAADF STEM images shown in (a) and (b)

The core electronic structure of Fe_3O_4-Pt was probed qualitatively via X-ray photoelectron spectroscopy (XPS). Pt ALD was performed using the same conditions for both a bare Si wafer substrate (control) and Fe_3O_4 superlattices deposited on a Si wafer substrate. Figure 5a shows the electron binding energy of Pt 4f determined from XPS for Pt NPs grown on a bare Si substrate. In comparison, we observe a ~0.4 eV decrease in the Pt 4f binding energy for Pt NPs grown on an Fe_3O_4 superlattice relative to Pt NPs grown on bare Si (see Figure 5b). This decrease in core electron binding energy corresponds to an increase in electron density in the Pt domain. Note that all spectra were calibrated to the C 1s reference peak at 284.5 eV to account for any charging effects, consistent with previous literature, and that the observed shift was reproducible over multiple experiments.[28] The shift in core electron density is likely due to charge transfer from Fe_3O_4 to the Pt domain, indicative of good electronic interaction between the Fe_3O_4 and Pt NPs. The Pt chemical shift by XPS has also been reported in thin film studies of the Pt/oxide interface,[29] indicating that metal-oxide-metal contact has been formed in the nanocomposite, a result which further highlights the benefits of our conceptual approach to the design and synthesis of supported catalysts.

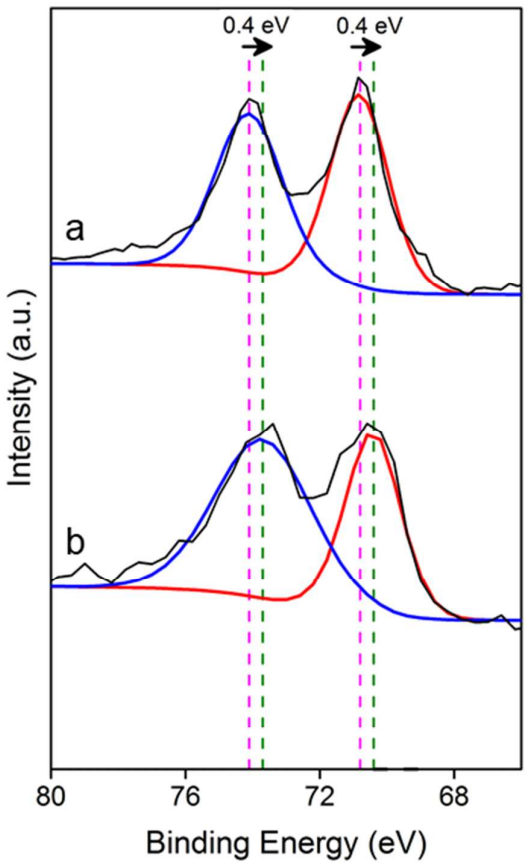

Figure 5. Pt 4f XPS spectra of Pt NPs (a) and Fe_3O_4-Pt nanocomposites (b) on Si substrates.

In order to further study the existence of charge transfer from Fe_3O_4 to Pt, photocurrent measurements were performed in an Ar-saturated 1 M NaOH electrolyte. Our electrode has been fabricated by electron beam depositing a Ag film followed by a TiO_2 film for ensuring good contact and stability during the O_2 plasma treatments for ALD. It can be seen in Figure 6 that the Fe_3O_4 in Fe_3O_4-Pt has a 2-fold enhancement in photocurrent intensity. This enhancement is due to the coupling of Fe_3O_4 NPs and Pt NPs, further proving the strong interaction through the Fe_3O_4-Pt interface. In order to confirm photoelectrocatalytic oxygen evolution reaction (OER) exists in this system, the current under chopped light was measured for sample Ag-TiO_2-Fe_3O_4-Pt with 200 ALD cycles at 0.2 V, showing the dark and light current could be constant for 10 seconds (See Figure S4). The dark current is very flat and close to zero, suggesting no redox reactions occur under the dark. In addition, the remarkable photocurrent at -0.2∽0.6 V (*VS Ag/AgCl*) (Figure 6) suggests that the photoelectrocatalytic activity is more likely related to OER.[30] However, the bare TiO_2 could couple with Pt for OER as well, and thus the photocurrent due to TiO_2-Pt coupling is strong for the TiO_2-Pt sample. Since our Fe_3O_4 almost fully covered the TiO_2 substrate, the dominant interaction for sample Fe_3O_4-Pt is from the Fe_3O_4-Pt nanocomposite, suggesting good electron transfer through the interface of Fe_3O_4 and Pt NPs. As Fe_3O_4 NPs are poor light absorbers compared to TiO_2 this led to slightly lower photocurrent intensity for Fe_3O_4-Pt coupling than TiO_2-Pt coupling. The incident to photon-to-current efficiency (IPCE) result showed in Figure S5 further confirmed that the Fe_3O_4-based composite has higher catalytic activity in the visible light range. However, due to the strong absorption of TiO_2 in the UV range, the overall photocurrent through a condenser lens (transmission: 350 nm – 700 nm) of TiO_2 based composite is slightly higher than Fe_3O_4 based composite. Further, the IPCE of Ag-TiO_2-Pt and Ag-TiO_2-Fe_3O_4-Pt with 250 cycles and 500 cycles of ALD showed the evidence for enhanced IPCE with more cycles (Figure S5 in SI). It should be noticed that Ag-TiO_2-Fe_3O_4-Pt with 250 cycles has higher intensity than Ag-TiO_2-Fe_3O_4-Pt with 500 cycles in UV range. This is probably due to the better coverage of TiO_2 on sample Ag-TiO_2-Fe_3O_4-Pt with 250 cycles, which mainly absorbs UV light. The higher intensity peak at 565 nm for Ag-TiO_2-Fe_3O_4-Pt with 500 cycles indicates the good interaction between Fe_3O_4 and Pt. The bump at 0.4 V was due to the oxidation of remaining organic ligands in the nanocomposites. Overall, decoration with Pt enhanced the activity of Fe_3O_4 NPs significantly, proving the efficient electron transfer from Fe_3O_4 to Pt NPs. The deposition of Pt forming Fe_3O_4-Pt nanocomposite induces significant improvement for Fe_3O_4 for photoelectrocatalysis. Additionally, this result corroborates our conclusions from the XPS study, providing further evidence of effective interphase charge transfer within the components of the Fe_3O_4-Pt superlattices. Long-duration durability testing was carried out on the photocurrent measurement (shown in Figure S6). The results indicated the system was active for more than 1000 s. The gradual decreasing of the intensity of the photocurrent might be due to the detachment of the Fe_3O_4-Pt from the substrate as the Fe_3O_4 has been deposited on the substrate through solution-based deposition method. However, achieving excellent stability of the photoelectrode is not the focus of this report; we plan future investigations on how to enhance stability such as functionalization of the surface of the substrate to form a strong bond between the substrate and NPs.

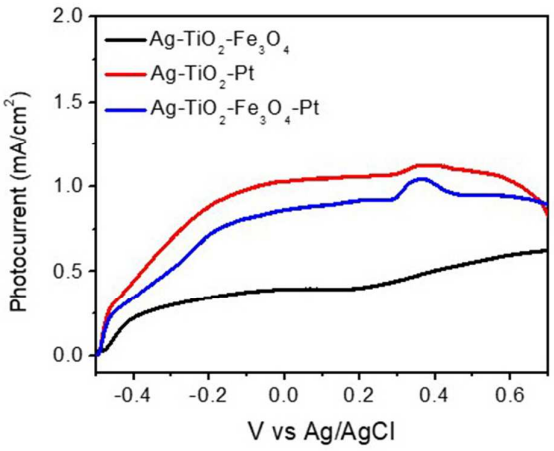

Figure 6. (a) Photocurrent measurements of Pt NPs (red), Fe_3O_4 NPs (black) and Fe_3O_4-Pt nanocomposites (blue) on the Ag-TiO_2 electrode. TiO_2 film (80 nm thick) was deposited on Ag thin film (100 nm thick) on a glass substrate.

Conclusions

In summary, we have developed Fe_3O_4-Pt superstructures by using a bottom-up colloidal synthesis and top-down ALD, resulting in controllable superstructure formation with good interaction between each components of the hybrids. In particular, good metal-oxide-metal contact has been formed by this design, which open a new avenue for tailoring of supported catalysts. Future work will be focused on using different metal oxide NPs as the oxide supports and systemically studying the influence of the Pt deposition on the photoelectrocatalysis.

Corresponding Author

*E-mail: jjurban@lbl.gov; a.a.bol@tue.nl.

Author Contributions

† F. Qiu and R. H. J. Vervuurt contributed equally to this work.

Conflicts of Interest

The authors declare no competing financial interests.

Acknowledgements

Work at the Molecular Foundry and the ALS was supported by the Office of Science, Office of Basic Energy Sciences, of the U.S. Department of Energy under Contract No. DE-AC02-05CH11231. The authors would like to thank C.O. van Bommel, C.A.A. van Helvoirt, J.J.L.M. Meulendijks & J.J.A. Zeebregts for technical assistance. This work is part of the research program of the Foundation for Fundamental Research on Matter (FOM), which is part of the Netherlands Organization for Scientific Research (NWO).

Notes and references

1. J. Yang, H. I. Elim, Q. B. Zhang, J. Y. Lee and W. Ji, *J Am Chem Soc*, 2006, **128**, 11921-11926.
2. R. Bliem, J. van der Hoeven, A. Zavodny, O. Gamba, J. Pavelec, P. E. de Jongh, M. Schmid, U. Diebold and G. S. Parkinson, *Angew. Chem. Int. Ed*, 2015, **54**, 13999-14002.
3. D. H. Wang, R. Kou, D. Choi, Z. G. Yang, Z. M. Nie, J. Li, L. V. Saraf, D. H. Hu, J. G. Zhang, G. L. Graff, J. Liu, M. A. Pope and I. A. Aksay, *Acs Nano*, 2010, **4**, 1587-1595.
4. S. Byun, Y. Song and B. M. Kim, *Acs Appl Mater Inter*, 2016, **8**, 14637-14647.
5. C. Wang, H. Daimon and S. H. Sun, *Nano Lett*, 2009, **9**, 1493-1496.
6. Z. M. Cui, G. T. Fu, Y. T. Li and J. B. Goodenough, *Angew. Chem. Int. Ed*, 2017, **56**, 9901-9905.
7. H. S. Wei, X. Y. Liu, A. Q. Wang, L. L. Zhang, B. T. Qiao, X. F. Yang, Y. Q. Huang, S. Miao, J. Y. Liu and T. Zhang, *Nat Commun*, 2014, **5**.
8. D. Ling, N. Lee and T. Hyeon, *Accounts Chem Res*, 2015, **48**, 1276-1285.
9. J. Park, K. J. An, Y. S. Hwang, J. G. Park, H. J. Noh, J. Y. Kim, J. H. Park, N. M. Hwang and T. Hyeon, *Nat. Mater*, 2004, **3**, 891-895.
10. Y. J. Kang, X. C. Ye, J. Chen, Y. Cai, R. E. Diaz, R. R. Adzic, E. A. Stach and C. B. Murray, *J Am Chem Soc*, 2013, **135**, 42-45.
11. T. Paik, B. T. Diroll, C. R. Kagan and C. B. Murray, *J Am Chem Soc*, 2015, **137**, 6662-6669.
12. A. J. M. Mackus, M. A. Verheijen, N. Leick, A. A. Bol and W. M. M. Kessels, *Chem Mater*, 2013, **25**, 1905-1911.
13. A. J. M. Mackus, M. J. Weber, N. F. W. Thissen, D. Garcia-Alonso, R. H. J. Vervuurt, S. Assali, A. A. Bol, M. A. Verheijen and W. M. M. Kessels, *Nanotechnology*, 2016, **27**.
14. B. J. O'Neill, D. H. K. Jackson, J. Lee, C. Canlas, P. C. Stair, C. L. Marshall, J. W. Elam, T. F. Kuech, J. A. Dumesic and G. W. Huber, *Acs Catal*, 2015, **5**, 1804-1825.
15. A. Pakkala and M. Putkonen, in *Handbook of Deposition Technologies for Films and Coatings (Third Edition)*, William Andrew Publishing, Boston, 2010, DOI:https://doi.org/10.1016/B978-0-8155-2031-3.00008-9, pp. 364-391.
16. A. J. M. Mackus, J. J. L. Mulders, M. C. M. van de Sanden and W. M. M. Kessels, *J Appl Phys*, 2010, **107**.
17. M. J. Weber, A. J. M. Mackus, M. A. Verheijen, C. van der Marel and W. M. M. Kessels, *Chem Mater*, 2012, **24**, 2973-2977.
18. M. W. Jiang, W. Liu, X. L. Yang, Z. Jiang, T. Yao, S. Q. Wei and X. G. Peng, *Acs Nano*, 2015, **9**, 10950-10960.
19. A. G. Dong, J. Chen, P. M. Vora, J. M. Kikkawa and C. B. Murray, *Nature*, 2010, **466**, 474-477.

20. M. S. Kumar, D. Chen, J. C. Walmsley and A. Holmen, *Catal Commun*, 2008, **9**, 747-750.
21. A. J. M. Mackus, N. Leick, L. Baker and W. M. M. Kessels, *Chem Mater*, 2012, **24**, 1752-1761.
22. V. I. Bukhtiyarov, B. L. Moroz, N. E. Bekk and I. P. Prosvirin, *Catalysis in Industry*, 2009, **1**, 17-28.
23. J. Chen, Q. H. Zhang, Y. Wang and H. L. Wan, *Adv Synth Catal*, 2008, **350**, 453-464.
24. A. Y. Stakheev, I. S. Mashkovskii, G. N. Baeva and N. S. Telegina, *Russ J Gen Chem+*, 2010, **80**, 618-629.
25. H. J. V. René, S. Akhil, J. Yuqing, M. M. K. Wilhelmus and A. B. Ageeth, *Nanotechnology*, 2016, **27**, 405302.
26. E. Farm, M. Kemell, M. Ritala and M. Leskela, *J Phys Chem C*, 2008, **112**, 15791-15795.
27. X. Jiang and S. F. Bent, *Journal of the Electrochemical Society*, 2007, **154**, D648-D656.
28. M. R. Buck, J. F. Bondi and R. E. Schaak, *Nat. Chem*, 2012, **4**, 37-44.
29. M. K. Bahl, S. C. Tsai and Y. W. Chung, *Phys Rev B*, 1980, **21**, 1344-1348.
30. X. D. Li, Z. Wang, Z. M. Zhang, L. L. Chen, J. L. Cheng, W. Ni, B. Wang and E. Q. Xie, *Sci Rep-Uk*, 2015, **5**.

TOC: